Li$_5$SnP$_3$ – a Member of the Series Li$_{10+4x}$Sn$_{2-x}$P$_6$ for $x=0$ Comprising the Fast Lithium-Ion Conductors Li$_8$SnP$_4$ ($x=0.5$) and Li$_{14}$SnP$_6$ ($x=1$)

Stefan Strangmüller,[a] David Müller,[a] Gabriele Raudaschl-Sieber,[b] Holger Kirchhain,[c] Leo van Wüllen,[c] and Thomas F. Fässler*[a]

Dedicated to Professor Richard Dronskowski on the occasion of his 60th birthday.

Abstract: The targeted search for suitable solid-state ionic conductors requires a certain understanding of the conduction mechanism and the correlation of the structures and the resulting properties of the material. Thus, the investigation of various ionic conductors with respect to their structural composition is crucial for the design of next-generation materials as demanded. We report here on Li$_5$SnP$_3$ which completes with $x=0$ the series Li$_{10+4x}$Sn$_{2-x}$P$_6$ of the fast lithium-ion conductors α- and β-Li$_8$SnP$_4$ ($x=0.5$) and Li$_{14}$SnP$_6$ ($x=1$). Synthesis, crystal structure determination by single-crystal and powder X-ray diffraction methods, as well as ^{6}Li, ^{31}P and ^{119}Sn MAS NMR and temperature-dependent ^{7}Li NMR spectroscopy together with electrochemical impedance studies are reported. The correlation between the ionic conductivity and the occupation of octahedral and tetrahedral sites in a close-packed array of P atoms in the series of compounds is discussed. We conclude from this series that in order to receive fast ion conductors a partial occupation of the octahedral vacancies seems to be crucial.

Introduction

Solid-state electrolytes (SE) are predicted to dominate mainly in electric vehicles and future lithium battery chemistry.[1] Therefore, extensive efforts are made aiming for the discovery of SE materials that are suitable to meet demanded properties for application in all-solid-state batteries.[2–4] Another approach focuses on a better understanding of the origin of materials' properties, such as ionic conductivity. The elaboration of structure-property relationships by comparison of a variety of crystalline candidate materials that comprise diverse structural differences with respect to their electronic properties allows for designing and tailoring of materials' properties as demanded.[5–8] Searching for high-performance ionic conductors, a large number of innovative SEs featuring ever increasing ionic conductivities has been reported over the last decades.[2–4,9,10] But a thorough investigation of structure-property relationships also demands the evaluation of less powerful materials in order to unveil the reasons for favorable or unfavorable properties.

The recently introduced family of lithium phosphidotetrelates and the closely related lithium phosphidotrielates are well-suited for further analyses of ionic conduction mechanisms as this class of materials offers a broad structural variety as well as a corresponding large variety of properties. For example, several compounds with a fast ionic conduction of up to 3×10^{-3} S cm^{-1} have been reported[3,4,7] next to materials that feature a band gap of about 3 eV, indicative of semiconducting behavior.[11] In addition the compound LiGe$_3$P$_3$ shows moderate electric conductivity and an unprecedented stability when exposed to water and air.[12] Apart from the latter and a few other exceptions, most of the so far discovered lithium phosphidotetrelates and -trielates are based on tetrahedral [TtP$_4$] or [TrP$_4$] units, which occur either as isolated [TtP$_4$]$^{8-}$ or [TrP$_4$]$^{9-}$ anions that are charge-compensated by the corresponding amount of Li$^+$ or they build frameworks of condensed tetrahedra and supertetrahedra, respectively.[8,11–15]

The compound Li$_{10}$Si$_2$P$_6$ comprises pairs of edge-sharing [SiP$_4$] units resulting in the polyanion [Si$_2$P$_6$]$^{10-}$.[16] Due to these building blocks, the formula is commonly given as Li$_{10}$Si$_2$P$_6$ rather than Li$_5$SiP$_3$ to express the molecular-anionic character.

[a] Dr. S. Strangmüller, D. Müller, Prof. Dr. T. F. Fässler
Department of Chemistry
Technische Universität München
Lichtenbergstraße 4, 85747 Garching bei München (Germany)
E-mail: Thomas.Faessler@lrz.tu-muenchen.de

[b] Dr. G. Raudaschl-Sieber
Department of Chemistry
Chair of Inorganic and Metal-Organic Chemistry
Technical University of Munich
Lichtenbergstraße 4, 85747 Garching bei München (Germany)

[c] Dr. H. Kirchhain, Prof. Dr. L. van Wüllen
Department of Physics
University of Augsburg
Universitätsstraße 1, 86159 Augsburg (Germany)

Chemistry–A European Journal

Research Article
doi.org/10.1002/chem.202104219

Chemistry
Europe
European Chemical
Societies Publishing

Indeed, a compound with the composition Li_5SiP_3 has been reported in the 1950s, and characterized by the determination of the cubic space group $Fm\bar{3}m$ with a lattice parameter of $a = 5.852$ Å.[17] The structure is closely related to the antifluorite type or a defect variant of the Li_3Bi structure,[18] which can be described by a ccp of P atoms in which all tetrahedral voids are statistically occupied by Li^+ and Si^{4+} in a mixing ratio of 5:1. So far, all attempts to reproduce these findings have failed.[13,16] However, about 20 years later the same structure was reported for the heavier homologue Li_5SnP_3[19] with identical cubic space group $Fm\bar{3}m$ (no. 225) and a lattice parameter of $a = 5.97$ Å. Further investigations of the material's properties are still pending, whereas the lithium-rich phosphidostannates α- and β-Li_8SnP_4 as well as $Li_{14}SnP_6$ have been recently reported to show superionic lithium-ion conductivities of about 1×10^{-3} S cm^{-1}. Interestingly in α- and β-Li_8SnP_4, the Li and Sn atoms are fully ordered in the tetrahedral voids of the ccp of P atoms, thus leading to polyanionic SnP_4^{8-} units. By contrast in $Li_{14}SnP_6$, the Li and Sn atoms are statistically distributed over the tetrahedral sites. Analysis of Li^+ diffusion pathways based on powder neutron diffraction data unveiled structural variations, which were directly connected to the different values of the ionic conductivities of the three compounds.[7,8]

In the following we report on the systematic investigation of the system $Li_{10+4x}Sn_{2-x}P_6$ ($x = 0.0$ to 1.0) including the compounds Li_5SnP_3, (α- and β-) Li_8SnP_4 and $Li_{14}SnP_6$ that arise for $x = 0.0$, 0.5, and 1.0, respectively. Following a well-established synthesis route for lithium phosphidotetrelates including mechano-chemical milling allows for the first time the isolation and detailed characterization of the compound Li_5SnP_3 by single-crystal and powder X-ray diffraction data completed by Rietveld refinement as well as ^6Li, ^{31}P and ^{119}Sn solid-state magic angle spinning (MAS) NMR measurements. Differential scanning calorimetry (DSC) and isothermal annealing experiments of the reactive mixtures obtained via mechanical alloying were carried out to investigate the thermal properties of the materials. Furthermore, the Li^+ mobility and its activation energy, as well as the ionic and electronic conductivity were determined via temperature-dependent ^7Li NMR spectroscopy and electrochemical impedance spectroscopy (EIS). Finally, all data and the associated properties are compared to that of the recently reported lithium phosphidostannates α- and β-Li_8SnP_4 and $Li_{14}SnP_6$, which allows for the formulation of new structure-property relationships regarding the ionic conductivity in solid-state Li^+ conductors.

Experimental Section

All syntheses were carried out under Ar atmosphere in glove boxes (MBraun, 200B) with moisture and oxygen levels below 0.1 ppm, or in containers, which were sealed under Ar atmosphere and vacuum ($<2 \cdot 10^{-2}$ mbar), respectively. Lithium phosphidostannates are sensitive to oxygen and moisture; in particular, contact with water results in a vigorous reaction including the formation of flammable and toxic gases (e.g., phosphine). Therefore, disposal must be addressed in small amounts at a time and under proper ventilation.

Bulk Synthesis via Ball Milling and Annealing: All samples were prepared by a well-established synthesis route starting from the elements, lithium (Rockwood Lithium, 99%), tin (Merck, 99.9%) and red phosphorus (ChemPUR, 99.999%) in stoichiometric amounts aiming for compositions according to the formula $Li_{10+4x}Sn_{2-x}P_6$ with $x = 0.00$, 0.25, 0.50, 0.75, 1.00 (Table 1), followed by annealing at moderate temperatures.

In the first step, a "reactive mixture" ($m = 5.0$ g) was prepared by mechano-chemical milling using a Retsch PM100 Planetary Ball Mill (350 rpm, 18 h, 10 min interval, 3 min break) with a tungsten carbide milling jar ($V = 50$ mL) and three balls with a diameter of 15 mm.

In the second step, the "reactive mixture" was pressed into pellets, sealed in batches of 0.3 to 1.0 g in carbon-coated silica glass ampules and heated in a muffle furnace (Nabertherm, L5/11/P330) to 673, 773 or 973 K (heating rate: 4 K min^{-1}) for 24 h, followed by quenching of the hot ampules in water.

Powder X-Ray Diffraction and Rietveld Refinement: Data were collected at room temperature on a STOE Stadi P diffractometer (Ge(111) monochromator, Cu$_{K\alpha1}$ radiation, $\lambda = 1.54056$ Å or Mo$_{K\alpha1}$ radiation, $\lambda = 0.70932$ Å) with a Dectris MYTHEN 1 K detector in Debye-Scherrer geometry. Samples were sealed in glass capillaries (Ø 0.3 mm) for measurement. Raw data were processed with the WinXPOW[20] software prior to refinement.

The data analysis of Li_5SnP_3 was performed using the full profile Rietveld method implemented in the FullProf program package.[21] To model the peak profile, the pseudo-Voigt function was chosen. The background contribution was determined using a linear interpolation between selected data points in non-overlapping regions. The scale factor, zero angular shift, profile shape parameters, resolution (Caglioti) parameters, asymmetry and lattice parameters as well as fractional coordinates of atoms and their displacement parameters were varied during the fitting. Free refinement of the occupancy of the 8c site by Sn and Li exhibited only marginal deviations from the electron-precise formula Li_5SnP_3 ($Z = 1.33$) or $Li_{6.67}Sn_{1.33}P_4$ ($Z = 1$). The corresponding data are given as Supporting Information. In addition, a second refinement was carried out with site occupancies set to the exact stoichiometry. Since the results of both refinements were in very good agreement, the electron precise stoichiometry Li_5SnP_3 is assumed. All structures were visualized using DIAMOND.[22]

Synthesis of powdery and single-crystalline Li_5SnP_3: Li_5SnP_3 is obtained as black powder on a gram scale and in high purity by annealing of the "reactive mixture" of the nominal composition "Li_5SnP_3" ($Li_{10+4x}Sn_{2-x}P_6$ with $x = 0.0$) in carbon-coated silica glass ampules at 773 K for 24 h, followed by quenching of the hot ampule in water. The weight fraction of remaining β-Sn was determined via Rietveld refinement to 0.8(1)%.

Single crystals were obtained by a high-temperature reaction of lithium (Rockwood Lithium, 99%), tin (Merck, 99.9%) and red phosphorus (Sigma-Aldrich, 97%) in a ratio corresponding to "Li_5SnP_6". The elements were annealed for 18 h at 873 K (heating

Table 1. Overview of the prepared "reactive mixtures" according to the formula $Li_{10+4x}Sn_{2-x}P_6$ ($x = 0.0$ to 1.0).

x	Composition
0.00	$Li_{10}Sn_2P_6 = Li_5SnP_3$
0.25	$Li_{11}Sn_{1.75}P_6$
0.50	$Li_{12}Sn_{1.5}P_6 = Li_8SnP_4$
0.75	$Li_{13}Sn_{1.25}P_6$
1.00	$Li_{14}SnP_6$

Chemistry–A European Journal

Research Article
doi.org/10.1002/chem.202104219

Chemistry Europe
European Chemical
Societies Publishing

rate: $4 \, K \, min^{-1}$) in a sealed tantalum ampule and subsequently quenched in water.

Single-crystal X-ray Diffraction Data Collection: A single crystal of Li_5SnP_3 was isolated and sealed in a glass capillary (0.1 mm). For diffraction data collection, the capillary was positioned in a 150 K cold N_2 gas stream. Data collection was performed with a STOE StadiVari ($Mo_{K\alpha1}$ radiation) diffractometer equipped with a DECTRIS PILATUS 300 K detector. Structures were solved by Direct Methods (SHELXS-2014) and refined by full-matrix least-squares calculations against F^2 (SHELXL-2014).[23]

Further details of the crystal structure investigations may be obtained from the joint CCDC/FIZ Karlsruhe online deposition service: Deposition Number(s) CSD-2074706 ($Li_{6.6667}Sn_{1.33}P_4$, single crystal), CSD-2074707 ($Li_{6.6667}Sn_{1.33}P_4$, powder), CSD-2074709 ($Li_{6.74}Sn_{1.29}P_4$, single crystal), and CSD-2074710 ($Li_{6.70}Sn_{1.30}P_4$, powder) contain(s) the supplementary crystallographic data for this paper. These data are provided free of charge by the joint Cambridge Crystallographic Data Centre and Fachinformationszentrum Karlsruhe Access Structures service.

Differential Scanning Calorimetry (DSC): The thermal behavior of the compounds was studied with a Netzsch DSC 404 Pegasus device. Niobium crucibles were filled with the samples and sealed by arc-welding. Empty sealed crucibles served as a reference. Measurements were performed under an Ar flow of $75 \, mL \, min^{-1}$ and a heating/cooling rate of $10 \, K \, min^{-1}$. Data collection and handling were carried out with the Proteus Thermal Analysis program,[24] and visualization was realized using OriginPro 2020.[25]

Solid-State NMR Spectroscopy: Magic angle spinning (MAS) NMR spectra were recorded on a Bruker Avance 300 NMR device operating at 7.04 T by the use of a 4 mm ZrO_2 rotor. The resonance frequencies of the measured nuclei are 44.2, 121.5 and 111.9 MHz for ^6Li, ^{31}P and ^{119}Sn, respectively. The rotational frequency was set to 15 kHz. The MAS spectra were acquired at room temperature with recycle delays of 10 to 30 s and 1000 to 2736 scans. All ^6Li spectra were referenced to LiCl (1 M, aq) and LiCl (s) offering chemical shifts of 0.0 ppm and -1.15 ppm, respectively. The ^{31}P spectra were referred to $(NH_4)H_2PO_4(s)$ (ammonium dihydrogen phosphate) with a chemical shift of 1.11 ppm with respect to concentrated H_3PO_4 (aq) (phosphoric acid). SnO_2 (s) (Cassiterite) was used as a secondary standard for the ^{119}Sn spectra, showing a chemical shift of -604.3 ppm[26,27] referred to $(CH_3)_4Sn(l)$ (tetramethylstannane). All spectra were recorded using single-pulse excitation.

Static ^7Li NMR experiments were performed using a Bruker Avance III spectrometer operating at a magnetic field of 7 T employing a 4 mm WVT MAS probe. The resonance frequency of the ^7Li nucleus is 116.6 MHz. The sample was sealed in a 4 mm glass tube to avoid contact with air and moisture. The temperature calibration for the measurements was performed using the temperature-dependent ^{207}Pb NMR shift of lead nitrate $(Pb(NO_3)_2)$ as chemical shift thermometer, which was also measured in a sealed glass tube. A saturation comb had been used prior to the ^7Li data acquisition. The spectra were recorded in the temperature range from room temperature to 200 K with recycle delays of 60 s and 4 scans. All spectra were referenced to LiCl (9.7 M, aq).

Impedance Spectroscopy and DC Conductivity Measurements: Potentiostatic impedance spectroscopy was carried out using a Biologic SP-300 potentiostat in a frequency range of 7 MHz to 100 mHz with an excitation amplitude of ± 10 mV. All measurements were conducted in an argon-filled glove box. Powder samples of Li_5SnP_3 (300 mg) were measured in a custom-built symmetric cell ($\varnothing = 8$ mm) with hardened steel electrodes under blocking conditions. Pressure was applied by six M14 screws, fastened with a defined torque of 30 Nm each, translating to proximately 480 MPa, so that the sample was compressed to 88% of its crystallographic density. A more detailed description can be found in the literature.[3] The temperature was controlled via a Julabo Dyneo DD 1000 Thermostat feeding an aluminum heating block, which enclosed the measurement cell. The electric conductivity was measured in the same cell setup with three polarization steps of 50, 100 and 150 mV, each held for 6 h to ensure equilibrium conditions.

Results

Syntheses

For the systematic investigation of lithium-rich ternary lithium phosphidostannates, mixtures with nominal compositions according to Table 1 were alloyed mechanically in a ball mill. The compositions were chosen according to the formula $Li_{10+4x}Sn_{2-x}P_6$ ($x = 0.0$ to 1.0) including also the compounds Li_5SnP_3,[19] α- and β-Li_8SnP_4,[8] as well as $Li_{14}SnP_6$[7] for $x = 0.0$, 0.5 and 1.0, respectively.
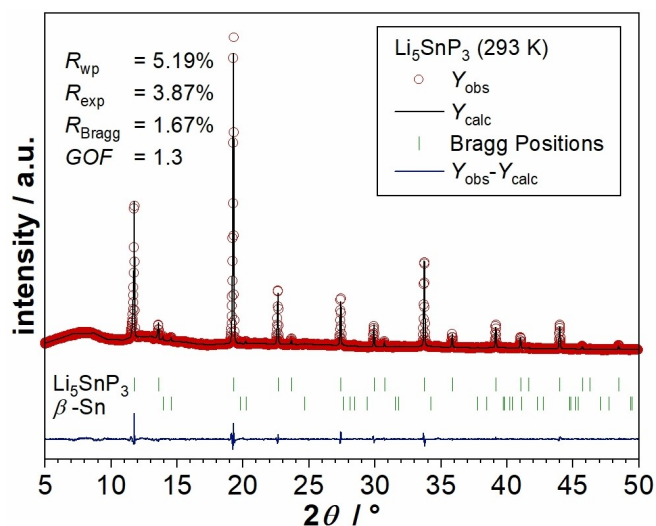
In order to detect further phases within this family of materials and to reveal existing phase widths of the compounds, the "reactive mixtures" were annealed at 673, 773 and 973 K, respectively. All "reactive mixtures" and products were analyzed using powder X-ray diffraction (PXRD) data for the identification of the occurring phases within the samples as well as for the determination of the cell parameters of the lithium phosphidostannates. The data showed the formation of the known compounds Li_5SnP_3,[19] α- and β-Li_8SnP_4[8] and $Li_{14}SnP_6$[7] as well as the presence of Li_3P and remaining β-Sn. Consequently, no phase widths were observed for these compounds. Details of the results and all PXRD patterns are given as Supporting Information.

For the structural reinvestigation of Li_5SnP_3 the corresponding "reactive mixture" obtained by ball milling of the elements in stoichiometric amounts was annealed at 773 K for 24 h, followed by quenching of the hot ampule in water. By this method, the material is accessible on a gram scale and in high purity as indicated by Rietveld analysis (Figure 1). Details of the refinement are shown in Table 2.

Differential scanning calorimetry, followed by PXRD measurements of the samples indicate the decomposition of Li_5SnP_3 at high temperatures, resulting in a mixture of β-Sn and another cubic phase, indicated by additional reflections assignable to a superstructure as observed for the ordered structures of α- and/ or β-Li_8SnP_4. Since the additional reflections are broadened, a partial ordering of the cations is assumed. The corresponding thermograms and PXRD patterns as well as a detailed discussion of the results is given as Supporting Information.

In accordance with previous reports,[19] the single-crystal data of Li_5SnP_3 indicate the cubic space group $Fm\bar{3}m$ (no. 225) and a lattice parameter of $a = 5.9541(7)$ Å at 150 K (Figure 2 and Table 3).

The structure of Li_5SnP_3 can be described as a *ccp* of P atoms (4*a* site) with the Sn and Li atoms statistically distributed in all tetrahedral voids (8*c* site) with a Sn:Li ratio of 1:5. The structure is thus closely related to the antifluorite structure with

Chemistry–A European Journal

Research Article
doi.org/10.1002/chem.202104219

Chemistry Europe
European Chemical
Societies Publishing

Figure 1. Results of the Rietveld analysis of the powder X-ray diffraction pattern of Li_5SnP_3 at 293 K. Red circles indicate observed intensities Y_{obs}, black lines show calculated intensities Y_{calc}, blue lines reveal the difference between observed and calculated intensities, and green marks indicate Bragg positions of Li_5SnP_3 (weight fraction 99(1) %) and β-Sn (weight fraction 0.8(1) %), respectively.
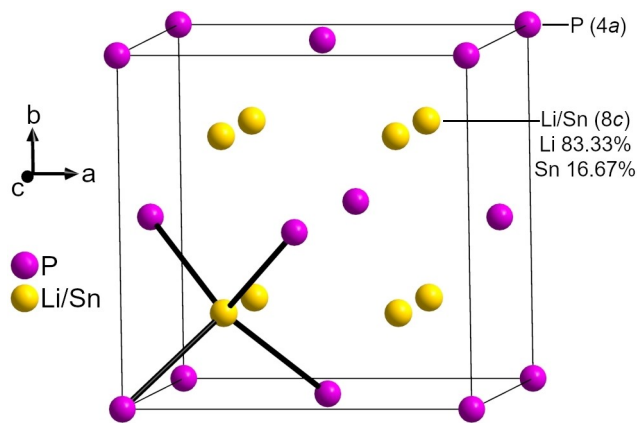

Figure 2. Structure of Li_5SnP_3 from single-crystal data at 150 K. P atoms (4a), and mixed Li/Sn sites (8c, Li 83.33 % and Sn 16.67 %) are depicted as pink and gold displacement ellipsoids, respectively, all set at 90 % probability. Black lines mark (Li/Sn)-P bonds, resulting in (Li/Sn)P_4 tetrahedra.
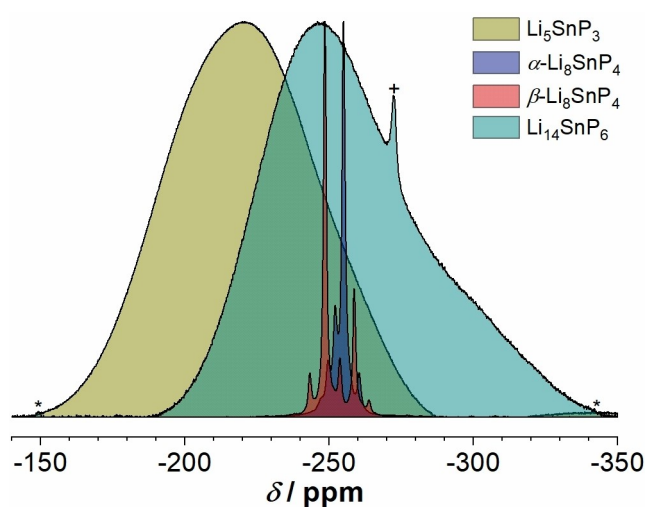
Table 2. Details of the Rietveld structure refinements of Li_5SnP_3 ($Z = 1.33$) at 293 K.

Empirical formula	$Li_{6.67}Sn_{1.33}P_4$
T [K]	293
formula weight [g mol^{-1}]	328.08
Group (no.)	$Fm\bar{3}m$ (225)
Unit cell parameters [Å]	$a = 5.98715(5)$
Z	1
V [Å^3]	214.615(3)
$\rho_{calc.}$ [g cm^{-3}]	2.541
2θ range [deg]	5.000–49.9441
R_p	3.87%
R_{wp}	5.19%
R_{exp}	3.87%
X^2	1.80
GOF	1.3
R_{Bragg}	1.67%
R_f	1.48%
Depository no.	CSD-2074707

Table 3. Crystallographic data and refinement parameters of Li_5SnP_3 ($Z = 1.33$) or $Li_{6.67}Sn_{1.33}P_4$ ($Z = 1$) at 150 K with fixed site occupancy factors.

empirical formula	$Li_5SnP_3/Li_{6.67}Sn_{1.33}P_4$
Formula weight [g mol^{-1}]	328.08
Crystal size [mm^3]	$0.08 \times 0.08 \times 0.09$
Crystal color	black
T [K]	150
Crystal system	cubic
Space group (no.)	$Fm\bar{3}m$ (225)
Unit cell parameter [Å]	$a = 5.9541(7)$
Z	0.75/1
V [Å^3]	211.08(7)
$\rho_{calc.}$ [g cm^{-3}]	2.583
μ [mm^{-1}]	4.644
$F(000)$ [e]	147
θ range [deg]	5.934–46.355
Index range (hkl)	$-7 \leq h \leq 11$, $-10 \leq k \leq 11$, $-11 \leq l \leq 4$
Reflections collected	348
Independent reflections	72
R_{int}	0.0101
Reflections with $I > 2\sigma(I)$	72
Absorption correction	multi-scan
Data/restraints/parameters	72/0/4
Goodness-of-fit on F^2	1.248
R_1, wR_2 (all data)	0.0231, 0.0231
R_1, wR_2 [$I > 2\sigma(I)$]	0.0626, 0.0626
Largest diff. peak and hole [e Å^{-3}]	0.968/−0.497
Depository no.	CSD-2074706

P and Li/Sn on Ca and F atom positions, respectively. The structure was also confirmed by powder X-ray diffraction and Rietveld refinement at 293 K. Atomic coordinates and anisotropic displacement parameters as well as the results from the powder X-ray diffraction at 293 K and the single-crystal X-ray diffraction at 150 K are given in the Supporting Information.

The structure of the lithium-rich compound $Li_{14}SnP_6$ is almost isotypic to that of Li_5SnP_3, but with a slightly larger lattice parameter ($a = 6.01751(3)$ Å) and a different occupation of the mixed Li/Sn positions in the tetrahedral voids and – due to the higher Li amount – partially occupied octahedral sites (4b). The same Li_3Bi-type structure was also observed for the lighter homologues $Li_{14}SiP_6$ and $Li_{14}GeP_6$.[3,7]

All interatomic Li/Sn–P (2.5782(2) Å), Li/Sn–Li/Sn (2.9771(3) Å) and P–P distances (4.2102(3) Å) are within the range of those found for related ternary or binary compounds like $Li_{14}TtP_6$ (Tt = Si, Ge, Sn),[3,7] (α-/β-)Li_8TtP_4 (Tt = Si, Ge, Sn)[8,13,14] and Li_3P.[28]

The ^{31}P MAS NMR spectrum of Li_5SnP_3 shows one very broad resonance (~17 kHz) at a chemical shift of −220.3 ppm (Figure S8). A comparable broadening was also observed in case of the structurally related and highly disordered compounds $Li_{14}TtP_6$ (Tt = Si, Ge, Sn).[3,7,29] Furthermore, it is assumed that the in some extend very complex coupling of Sn and P atoms also leads to a merging of signals with a related chemical shift as recently reported for example, for α- and β-Li_8SnP_4.[8] In

Chemistry–A European Journal

Research Article
doi.org/10.1002/chem.202104219

Chemistry Europe
European Chemical
Societies Publishing

comparison to the resonances of the latter and of other closely related lithium phosphidostannates such as $Li_{14}SnP_6$,[7] the maximum of the signal appertaining to Li_5SnP_3 shows a downfield shift of about 20 to 40 ppm. This indicates a lower shielding of the P atoms and hints for a lower formal charge (< -2) and to a higher coordination number of P by Sn atoms (Figure 3). At the local level, all P atoms in Li_5SnP_3 are covalently bound to at least one Sn atom, whereas in $Li_{14}TtP_6$ also P^{3-} anions are present according to $[(Li^+)_{14}(TtP_4)^{8-}(P^{3-})_2]$. In analogy to the structures of α- and β-Li_8SnP_4 and $Li_{14}SnP_6$, respectively, the Sn atoms are occupying tetrahedral voids, resulting in SnP_4 units.[7,8] Regarding the electron-precise stoichiometry (Li_5SnP_3 or $Li_{6.67}Sn_{1.33}P_4$), each P atom is statistically coordinated by 1.33 Sn atoms. Thus, one would expect the coordination of 1/3 of all P atoms by two Sn atoms, and all the others coordinate to one
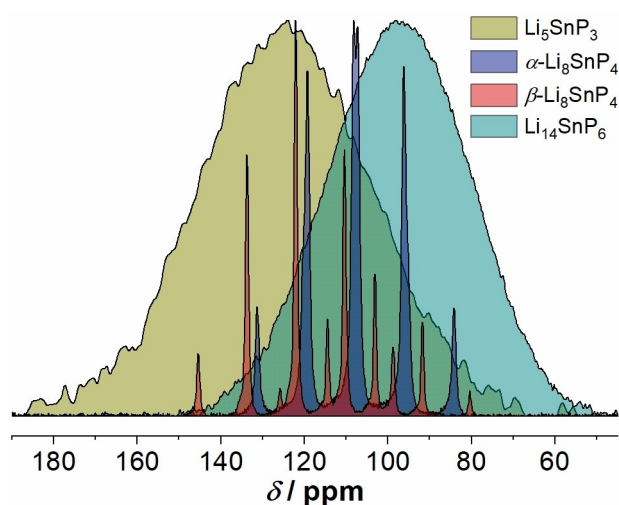
Sn atom. In other words, two Sn atoms occupy adjacent tetrahedral voids and form edge-sharing tetrahedra with the formula $[Sn_2P_6]^{10-}$. Such units are also observed in the homologous lithium phosphidosilicate $Li_{10}Si_2P_6$.[16] However, the $[Sn_2P_6]^{10-}$ units are not ordered, and thus, the chemically different P atoms do not appear with a distinct difference in the chemical environment. A further resolution of the broad signal in order to distinguish P atoms located next to only one Sn atom (1b-P^{2-}) and P atoms surrounded by two Sn atoms (2b-P^{1-}) was not feasible. Possible reasons are given after the discussion of the ^{119}Sn NMR spectrum.

Regarding the ^{119}Sn NMR spectrum of Li_5SnP_3, the high level of cation disorder also results in only one very broad (~ 13 kHz) tin resonance at a chemical shift of 124.6 ppm (Figure S9). In analogy to the ^{31}P NMR measurements, this effect has also been observed in the ^{119}Sn spectrum of $Li_{14}SnP_6$.[7] In comparison to the latter, the maximum of the signal for Li_5SnP_3 shows a downfield shift of 26.5 ppm, and the resonances of the lithium phosphidostannates Li_5SnP_3, α- and β-Li_8SnP_4 and $Li_{14}SnP_6$ shown in Figure 4 are upfield shifted depending on the Sn to P ratio indicating the slightly different bonding situations within the compounds discussed above.[7,8]

Regarding the electron-precise stoichiometry of the so far known lithium phosphidostannates the structure of $Li_{14}SnP_6$ shows both, $[SnP_4]^{8-}$ and P^{3-} units, whereas the two modifications of Li_8SnP_4 only contain $[SnP_4]^{8-}$ tetrahedra, and the basic structure of Li_5SnP_3 consists of $[Sn_2P_6]^{10-}$ units.[7,8] This, in combination with the crystal structures and the just discussed NMR data, at first appears counterintuitively since neither the NMR data nor the crystallographic data clearly resolve the presence of edge-sharing $[SnP_4]$ tetrahedra in Li_5SnP_3, which are correspondingly reported for $Li_{10}Si_2P_6$. In contrast to the strongly covalent character of the Si–P bonds leading to molecule-like $[Si_2P_6]$ units[16] the bonding situation in Li_5SnP_3 is assumed to be mainly dominated by the ionic character of the Sn–P bonds resulting in much weaker bonds and, thus, in more uniform chemical environments.

The ^{6}Li MAS NMR spectrum shows only one signal corresponding to the one Li site in the structure. The chemical shift of $\delta = 4.2$ ppm occurs within the characteristic range of ^{6}Li resonances reported for lithium phosphidotetrelates and -trielates.[3,4,7,8,11–14,16]

Lithium-ion mobility
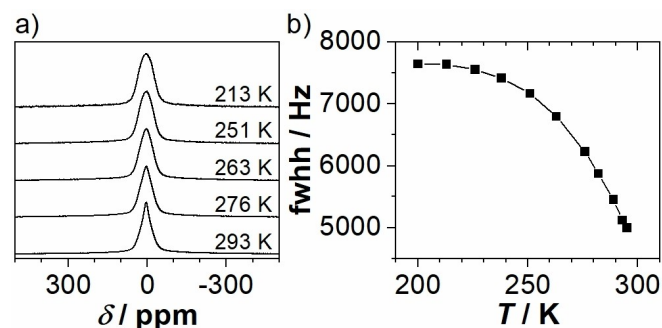
The Li^+ mobility, the activation energy and the ionic as well as the electronic conductivity are evaluated and compared to recent results of the related compounds α- and β-Li_8SnP_4 and $Li_{14}SnP_6$.

For a rough estimation of the activation barrier for Li^+ mobility in crystalline Li_5SnP_3 the dynamic behavior of Li^+ was investigated by temperature-dependent evolution of the static ^{7}Li NMR line width. Since the central transition of the $I = 3/2$ ^{7}Li nucleus is broadened by homonuclear (^{7}Li–^{7}Li) and heteronuclear (^{7}Li–^{31}P) dipolar coupling, both of which scale with the second Legendrian (3 $\cos^2 \beta$-1), any dynamic process leads to a

Figure 3. Overview of the ^{31}P MAS NMR spectra of Li_5SnP_3 (olive), α-Li_8SnP_4 (blue), β-Li_8SnP_4 (red),[8] and $Li_{14}SnP_6$ (teal).[7] Spinning sidebands and Li_3P (impurity) are indicated by * and +, respectively.

Figure 4. Overview of the ^{119}Sn MAS NMR spectra of Li_5SnP_3 (olive), α-Li_8SnP_4 (blue), β-Li_8SnP_4 (red),[8] and $Li_{14}SnP_6$ (teal).[7]

Chemistry–A European Journal

Research Article
doi.org/10.1002/chem.202104219

Chemistry Europe
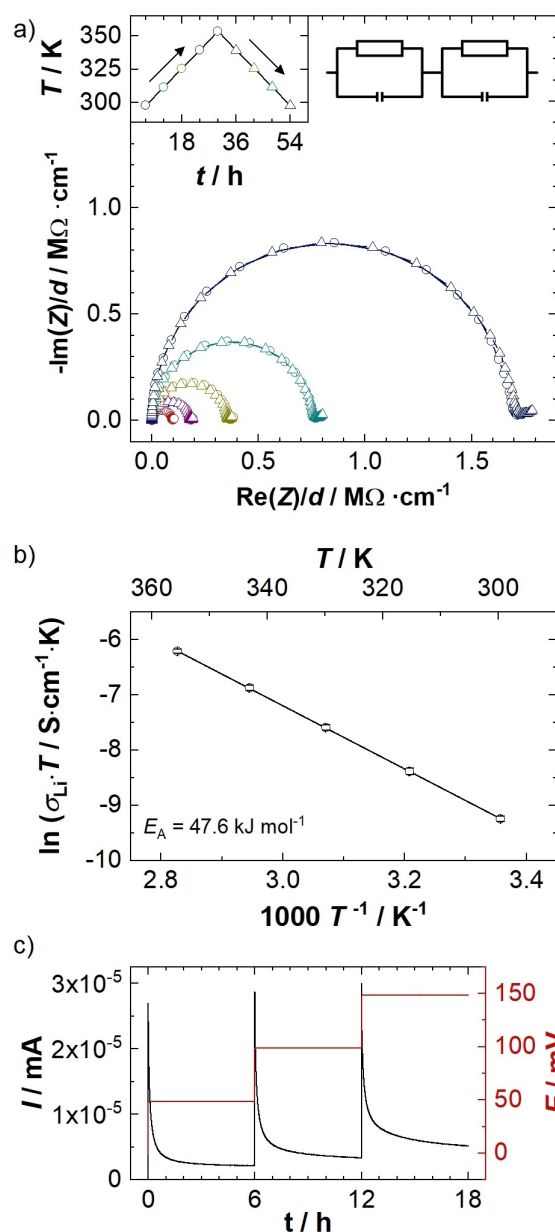European Chemical
Societies Publishing

(partial) averaging of this orientational dependence and, thus, to a narrowing of the NMR line. The corresponding results are depicted in Figure 5. At 213 K a single Gaussian line was obtained at 3.9 ppm with a line width of about 7.6 kHz. At temperatures above 263 K the signal becomes more heterogeneous and increasingly Lorentz-shaped, combined with a stronger narrowing of the line. The resonance remains heterogeneous up to 300 K, with a line width of 5.0 kHz. Application of the empirical Waugh-Fedin relation, $E_A^{NMR} = 0.156 \cdot T_{onset}$[30] allows for a rough estimation of the activation energy. Since the high-temperature plateau is not reached at 300 K an activation energy of $E_A^{NMR} = 47$ kJ mol^{-1} or higher can be assumed.

In comparison with the corresponding values determined for the lithium-richer phosphidostannates α- and β-Li$_8$SnP$_4$ ($E_A^{NMR} = 34$ and 28 kJ mol^{-1}, respectively) and Li$_{14}$SnP$_6$ ($E_A^{NMR} = 28$ kJ mol^{-1}) the estimated activation energy for Li$_5$SnP$_3$ is by far the highest. Moreover, since the onset temperature T_{onset} is estimated to be at 300 K or higher, no or only an extremely low conductivity is expected in electrochemical impedance measurements.

The ionic conductivity of Li$_5$SnP$_3$ was determined by electrochemical impedance spectroscopy (EIS) in a blocking electrode configuration. The results obtained at temperatures between 298 and 353 K± 0.5 K are shown in Figure 6a. The Nyquist plots exhibit well resolved but slightly broadened semicircles and the onset of a branch at low frequencies. For the evaluation of the ionic conductivity only the high-frequency semicircle was fitted, using two serial R/C elements, revealing two processes involved in the ionic conduction mechanism, that is, a dominant process with a capacity of $3(5) \cdot 10^{-10}$ F and a minor process with a capacitance of $5(1) \cdot 10^{-7}$ F. The first process can be assigned, according to Irvine et al.,[31] to grain boundary-controlled ionic conductivity, while the latter resembles the contribution of a surface layer. The overall ionic conductivity at 298 K was determined to $3.2(2) \cdot 10^{-7}$ S cm^{-1}. Calculated from the slope of the Arrhenius plot in Figure 6b, the activation energy of the ionic mobility was determined to $E_A^{PEIS} = 47.6(6)$ kJ mol^{-1} (~ 0.49 eV). The electric conductivity of the sample was studied by polarization of the sample in three different potential steps of 50, 100 and 150 mV, each held until stationary conditions were approached, monitoring the current in the same cell setup

Figure 6. a) Nyquist plot of Li$_5$SnP$_3$ measured under blocking conditions, with spectra recorded at temperatures between 298 and 353 K according to the color code of the inset. Circles and triangles indicate data collection during heating and cooling, respectively. The equivalent circuit used for fitting is also shown; b) Arrhenius plot of the product of conductivity and temperature ($\sigma_{Li} T$) obtained in one heating-cooling cycle, with error bars for each temperature based on the standard deviation from independent measurements with three cells; the shown linear fit was used to obtain the activation energy E_A^{PEIS}; c) polarization curves of Li$_5$SnP$_3$ for the determination of the electronic conductivity. The black line referring to the left y axis shows the recorded current, while the red line (right y axis) shows the applied potential steps.

Figure 5. a) Static ^{7}Li spectra of Li$_5$SnP$_3$ at various temperatures; b) evolution of the ^{7}Li line width in the temperature range from 200 K to room temperature for Li$_5$SnP$_3$. The solid line only serves as a guide to the eye.

as for impedance spectroscopy (Figure 6c). Application of Ohm's law results in an electronic conductivity of $2.1(9) \cdot 10^{-8}$ S cm^{-1}, which is approximately one order of magnitude lower than the ionic conductivity.

Chemistry–A European Journal

Research Article
doi.org/10.1002/chem.202104219

**Chemistry Europe**
European Chemical
Societies Publishing

Discussion and Conclusion

The straightforward synthesis of single crystals and phase-pure microcrystalline powders finally allows for a comparison of the structure and properties of Li_5SnP_3 with that of the recently reported compounds α- and β-Li_8SnP_4 and $Li_{14}SnP_6$, which contain an increasing percentage of Li^+.[7,8] On both the Li-poor and Li-rich sides, mixed Li/Sn positions in a small cubic unit cell occur. The cell parameters shown in Table 4 increase with a higher content of Li^+ because the exchange of one Sn^{4+} requires the insertion of four Li^+ to keep the electronic preciseness of the structures. The relatively small amount of Li^+ in Li_5SnP_3 is found to occupy all tetrahedral voids, whereas the octahedral voids remain completely empty, and thus, the octahedral voids must be regarded as energetically less favored. With increasing Li^+ content, however, also the octahedral voids are progressively filled reaching an occupancy of 25% in α- and β-Li_8SnP_4 and of 50% in $Li_{14}SnP_6$.

In addition, Figure 7 reveals a correlation between the occupancy of the octahedral voids and the ionic conductivity, and the latter increases from Li_5SnP_3 to $Li_{14}SnP_6$ by more than three orders of magnitude. The relatively low ionic conductivity of Li_5SnP_3 is attributed to the absence of occupied octahedral voids and corroborates the assumption that these vacancies are energetically less favored. As a consequence, Li^+ diffusion does not occur via octahedral sites but through edge-sharing tetrahedral voids that require a higher activation energy if compared to the diffusion along face-sharing tetrahedral and octahedral voids, as recently shown by the investigation of Li^+ diffusion pathways in α- and β-Li_8SnP_4 and $Li_{14}SnP_6$.

The systematic investigation of the ternary Li/Sn/P system within the formula $Li_{10+4x}Sn_{2-x}P_6$ ($x = 0.0$ to 1.0) did not lead to compounds with other Li/Sn ratios than that of the previously reported phases Li_5SnP_3,[19] α- and β-Li_8SnP_4[8] and $Li_{14}SnP_6$.[7] Interestingly, no ordered structure is observed for Li_5SnP_3 and $Li_{14}SnP_6$, whereas two polymorphs with distinctly ordered cation positions are found for the Li_8SnP_4. In addition, there is no evidence of a phase width of the compounds. The disorder in Li_5SnP_3 and $Li_{14}SnP_6$ is in accordance with the recorded ^{31}P and ^{119}Sn MAS NMR spectra, which exhibit extremely broad resonances. Such broad resonances hint for a vague chemical environment of the P and Sn atoms. Nevertheless, the chemical shift of the signals is within the range of the resonances reported for the ordered structures of α- and β-Li_8SnP_4, indicating the presence of $[SnP_4]$ tetrahedra in Li_5SnP_3, which in accordance with the charge are expected to form edge-sharing $[Sn_2P_6]^{10-}$ dimers as found as ordered variant in $Li_{10}Si_2P_6$.[16]

A two-step synthesis route, including mechanical alloying and subsequent annealing of the samples, yields all four compounds in high purity and on a gram scale allowing for a profound determination of the properties.

The low ionic conductivity of $\sigma_{Li} = 3.2(2) \cdot 10^{-7}\,S\,cm^{-1}$ of Li_5SnP_3 in combination with vacant octahedral sites on the one hand, and the high ionic conductivity of α- and β-Li_8SnP_4 as well as of $Li_{14}SnP_6$ with partially filled octahedral sites on the other unequivocally proof the importance of the participation of the octahedral voids in ion motion. In order to lower the activation energy one can either lower the energy barrier for Li^+ motion between neighboring sites or raise the energy level of the respective sites. The partial occupation of the energetically unfavorable octahedral voids in the Li-rich phosphidotetrelates corresponds to the latter case and leads to an overall flattening of the energy landscape. In this context the investigation of less promising Li^+-conducting materials with insufficient ionic conductivities for application, plays a key role in the understanding of the criteria to design and tailor next-generation ionic conductors.

Supporting Information Summary

Details of crystal structure determination of Li_5SnP_3, details on the investigation of the system $Li_{8-4x}Sn_{1+x}P_4$ ($x = -0.333$ to $+0.333$), differential scanning calorimetry (DSC), ^6Li, ^{119}Sn, and ^{31}P MAS NMR spectroscopy.

Acknowledgements

Table 4. Comparison of the cell parameter a, the ionic and electronic conductivities σ_{Li} and σ_{el} and the activation energy E_A^{PEIS} of the lithium phosphidostannates Li_5SnP_3, α- and β-Li_8SnP_4 and $Li_{14}SnP_6$ at ambient temperature.

empirical formula	Li_5SnP_3	α-Li_8SnP_4	β-Li_8SnP_4	$Li_{14}SnP_6$
a [Å] ($\frac{a}{2}$ [Å])	5.98715	11.97626 (5.98813 Å)	11.99307 (5.996535 Å)	6.01751
σ_{Li} [$S\,cm^{-1}$]	$3.2 \cdot 10^{-7}$	$1.2 \cdot 10^{-4}$	$6.6 \cdot 10^{-4}$	$9.3 \cdot 10^{-4}$
σ_{el} [$S\,cm^{-1}$]	$2.1 \cdot 10^{-8}$	$1.4 \cdot 10^{-7}$	$6.1 \cdot 10^{-7}$	$4.1 \cdot 10^{-7}$
E_A^{PEIS} [$kJ\,mol^{-1}$]	47.6	36.0	32.4	33.8
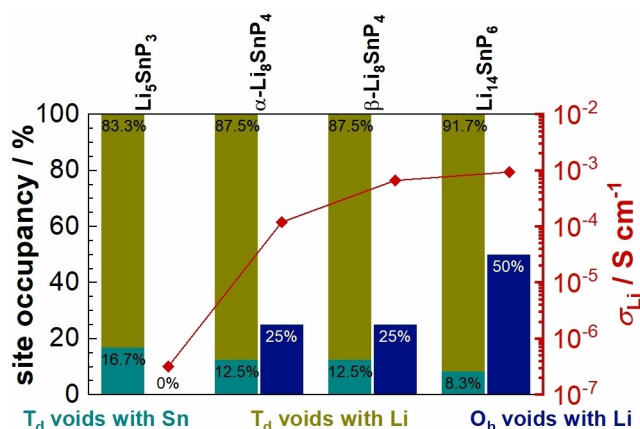
Figure 7. Correlation between the occupation of the tetrahedral and octahedral voids and the resulting ionic conductivity of the phases Li_5SnP_3, α- and β-Li_8SnP_4 and $Li_{14}SnP_6$. The percentages of Sn and Li in the tetrahedral voids are shown in teal and olive, respectively, and the partial occupation of the octahedral voids is indicated in blue. The corresponding ionic conductivity at room temperature is shown in red according to the scale on the right.

Chem. Eur. J. **2022**, *28*, e202104219 (7 of 8)

© 2021 The Authors. Chemistry - A European Journal published by Wiley-VCH GmbH

Chemistry–A European Journal

Research Article
doi.org/10.1002/chem.202104219

Chemistry
Europe
European Chemical
Societies Publishing

Conflict of Interest

The authors declare no conflict of interest.

Data Availability Statement

The data that support the findings of this study are available in the supplementary material of this article.

[1] Y. Horowitz, C. Schmidt, D.-h. Yoon, L. M. Riegger, L. Katzenmeier, G. M. Bosch, M. Noked, Y. Ein-Eli, J. Janek, W. G. Zeier, C. E. Diesendruck, D. Golodnitsky, *Energy Technol.* **2020**, *8*, 2000580.
[2] Y. Kato, S. Hori, T. Saito, K. Suzuki, M. Hirayama, A. Mitsui, M. Yonemura, H. Iba, R. Kanno, *Nat. Energy* **2016**, *1*, 16030.
[3] S. Strangmüller, H. Eickhoff, D. Müller, W. Klein, G. Raudaschl-Sieber, H. Kirchhain, C. Sedlmeier, V. Baran, A. Senyshyn, V. L. Deringer, L. van Wüllen, H. A. Gasteiger, T. F. Fässler, *J. Am. Chem. Soc.* **2019**, *141*, 14200–14209.
[4] T. M. F. Restle, C. Sedlmeier, H. Kirchhain, W. Klein, G. Raudaschl-Sieber, V. L. Deringer, L. van Wüllen, H. A. Gasteiger, T. F. Fässler, *Angew. Chem. Int. Ed.* **2020**, *59*, 5665–5674; *Angew. Chem.* **2020**, *132*, 5714–5723.
[5] S. P. Culver, R. Koerver, T. Krauskopf, W. G. Zeier, *Chem. Mater.* **2018**, *30*, 4179–4192.
[6] S. Ohno, A. Banik, G. F. Dewald, M. A. Kraft, T. Krauskopf, N. Minafra, P. Till, M. Weiss, W. G. Zeier, *Prog. Energy* **2020**, *2*, 022001.
[7] S. Strangmüller, H. Eickhoff, G. Raudaschl-Sieber, H. Kirchhain, C. Sedlmeier, L. van Wüllen, H. A. Gasteiger, T. F. Fässler, *Chem. Mater.* **2020**, *32*, 6925–6934.
[8] S. Strangmüller, H. Eickhoff, W. Klein, G. Raudaschl-Sieber, H. Kirchhain, T. Kutsch, V. Baran, A. Senyshyn, L. van Wüllen, H. A. Gasteiger, T. F. Fässler, *J. Mater. Chem. A* **2021**, *9*, 15254–15268.
[9] N. Kamaya, K. Homma, Y. Yamakawa, M. Hirayama, R. Kanno, M. Yonemura, T. Kamiyama, Y. Kato, S. Hama, K. Kawamoto, A. Mitsui, *Nat. Mater.* **2011**, *10*, 682–686.
[10] H.-J. Deiseroth, S.-T. Kong, H. Eckert, J. Vannahme, C. Reiner, T. Zaiß, M. Schlosser, *Angew. Chem. Int. Ed.* **2008**, *47*, 755–758; *Angew. Chem.* **2008**, *120*, 767–770.
[11] T. M. F. Restle, J. V. Dums, G. Raudaschl-Sieber, T. F. Fässler, *Chem. Eur. J.* **2020**, *26*, 6812–6819.
[12] H. Eickhoff, C. Sedlmeier, W. Klein, G. Raudaschl-Sieber, H. A. Gasteiger, T. F. Fässler, *Z. Anorg. Allg. Chem.* **2020**, *646*, 95–102.
[13] L. Toffoletti, H. Kirchhain, J. Landesfeind, W. Klein, L. van Wüllen, H. A. Gasteiger, T. F. Fässler, *Chem. Eur. J.* **2016**, *22*, 17635–17645.
[14] H. Eickhoff, S. Strangmüller, W. Klein, H. Kirchhain, C. Dietrich, W. G. Zeier, L. van Wüllen, T. F. Fässler, *Chem. Mater.* **2018**, *30*, 6440–6448.
[15] A. Haffner, T. Bräuniger, D. Johrendt, *Angew. Chem. Int. Ed.* **2016**, *55*, 13585–13588; *Angew. Chem.* **2016**, *128*, 13783–13786.
[16] H. Eickhoff, L. Toffoletti, W. Klein, G. Raudaschl-Sieber, T. F. Fässler, *Inorg. Chem.* **2017**, *56*, 6688–6694.
[17] R. Juza, W. Schulz, *Z. Anorg. Allg. Chem.* **1954**, *275*, 65–78.
[18] E. Zintl, G. Brauer, *Z. Elektrochem.* **1935**, *41*, 297–303.
[19] A. El Maslout, J.-P. Motte, C. Gleitzer, *J. Solid State Chem.* **1973**, *7*, 250–254.
[20] WinXPOW 3.0.2.1, STOE & Cie GmbH, Darmstadt, Germany, **2011**.
[21] J. Rodriguez-Carvajal, J. Gonzales-Platas, *Fullprof*, Institute Laue-Langevin Grenoble, France, **2020**.
[22] K. Brandenburg, Crystal Impact GbR, Bonn, Germany, **2014**.
[23] G. M. Sheldrick, *Acta Crystallogr. Sect. C* **2015**, *71*, 3–8.
[24] Netzsch-Gerätebau GmbH, Selb, **2006**.
[25] OriginLab Corporation, Northampton, MA, USA, **2020**.
[26] N. J. Clayden, C. M. Dobson, A. Fern, *J. Chem. Soc. Dalton Trans.* **1989**, 843–847.
[27] M. R. Mitchell, S. W. Reader, K. E. Johnston, C. J. Pickard, K. R. Whittle, S. E. Ashbrook, *Phys. Chem. Chem. Phys.* **2011**, *13*, 488–497.
[28] Y. Dong, F. J. DiSalvo, *Acta Crystallogr. Sect. E* **2007**, *63*, i97–i98.
[29] D. Franke, C. Hudalla, R. Maxwell, H. Eckert, *J. Phys. Chem.* **1992**, *96*, 7506–7509.
[30] J. S. Waugh, E. I. Fedin, *Soviet Physics-Solid State* **1963**, *4*, 1633–1636.
[31] J. T. S. Irvine, D. C. Sinclair, A. R. West, *Adv. Mater.* **1990**, *2*, 132–138.